Title

Application of the Grasshopper Optimization Algorithm (GOA) to the Optimal Operation of Hydropower Reservoir Systems Under Climate Change

Journal

Water Resources Management, 35(13)

ISSN

0920-4741

Authors

Rahmati, Kobra
Ashofteh, Parisa-Sadat
Loáiciga, Hugo A

Publication Date

2021-10-01

DOI

10.1007/s11269-021-02950-z

Peer reviewed

Water Resources Management (2021) 35:4325–4348
https://doi.org/10.1007/s11269-021-02950-z

Application of the Grasshopper Optimization Algorithm (GOA) to the Optimal Operation of Hydropower Reservoir Systems Under Climate Change

Kobra Rahmati[1] · Parisa-Sadat Ashofteh[1] · Hugo A. Loáiciga[2]

Received: 22 April 2021 / Accepted: 17 August 2021 / Published online: 24 September 2021

Abstract
Hydropower is a low-carbon energy source, which may be adversely impacted by climate change. This work applies the Grasshopper Optimization Algorithm (GOA) to optimize hydropower multi-reservoir systems. Performance of GOA is compared with that of particle swarm optimization (PSO). GOA is applied to hydropower, three-reservoir system (Seymareh, Sazbon, and Karkheh), located in the Karkheh basin (Iran) for baseline period 1976–2005 and two future periods (2040–2069) and (2070–2099) under greenhouse gases pathway scenarios RCP2.6, RCP4.5, and RCP8.5. GOA minimizes the shortage of hydropower energy generation. Results from GOA optimization of Seymareh reservoir show that average objective function in baseline is 85 and minimum value of average objective function in 2040–2069 would be under RCP2.6 (equal to 0.278). Optimization of Seymareh-reservoir based on PSO shows that average value of objective function in baseline is less (that is, better) than value obtained with GOA (10.953). Optimization results for two-reservoir system (Sazbon and Karkheh) based on GOA optimization show that objective function in baseline is 5.44 times corresponding value obtained with PSO, standard deviation is 2.3 times that calculated with PSO, and run-time is 1.5 times PSO's. Concerning three-reservoir systems it was determined that objective function based on PSO had the best value (the lowest energy deficit), especially in future. GOA converges close to the best objective function, especially in future-periods optimization, and convergence to solutions is more stable than PSO's. A comparison of performance of GOA and PSO indicates PSO converges faster to optimal solution, and produces better objective function than GOA.

Keywords Grasshopper optimization algorithm · Climate change · Hydropower multi-reservoir system · Particle swarm algorithm

✉ Parisa-Sadat Ashofteh
PS.Ashofteh@qom.ac.ir

Kobra Rahmati
k.rahmati@stu.qom.ac.ir

Hugo A. Loáiciga
hloaiciga@ucsb.edu

[1] Department of Civil Engineering, University of Qom, Qom, Iran

[2] Department of Geography, University of California, Santa Barbara, CA 93016-4060, USA

1 Introduction

Hydropower constitutes a source of clean and renewable energy under suitable conditions. Operation of hydropower multi-reservoir systems under climate change guided by meta-heuristic algorithms offers opportunities for improvement compared with rule-based empirical policies. Numerous methods have been used to optimize hydropower generation. For example, Hosseini-Moghari et al. (2015) used Imperialist Competitive Algorithm (ICA) and Cuckoo Optimization Algorithm (COA) to optimally operate Karun-4 reservoir (Iran) with aim of maximizing productivity. Bozorg-Haddad et al. (2016) applied Biogeography-Based Optimization (BBO) to single- and four-reservoir systems operation. Their results showed superiority of BBO over Genetic Algorithm (GA) in achieving optimal global solutions. Garousi-Nejad et al. (2016b) implemented Firefly Algorithm (FA) for optimal operation of Karun-4 reservoir (Iran) for agricultural water supply and hydropower generation purposes. Bozorg-Haddad et al. (2017) evaluated performance of an extended multi-objective developed firefly algorithm (MODFA) for hydropower energy generation. Ahmadianfar et al. (2017) introduced Enhanced Differential Evolution (EDE) to improve Differential Evolution (DE) Algorithm. Their results indicated high effectiveness of EDE for solving complex multi-reservoir problems. Chang et al. (2018) proposed a method consisting of simulation and optimization models to identify operating rules in a hydropower plant on Hanjian river (China) under climate change. Sarzaeim et al. (2018) applied non-dominated sorting genetic algorithm (NSGA-II) to maximize simultaneous annual hydropower generation and power plant coefficient under climate change in Karkheh river Iran. Fallah-Mehdipour et al. (2018) calculated multi-objective optimal tradeoffs between environmental flows and hydropower generation with optimization tool of fixed length gene genetic programming (FLGGP). Zhang et al. (2019) reported use of analytical methods for optimal hydropower generation in multi-reservoir systems. Ahmadianfar et al. (2019) applied multiple linear rules for multi-reservoir hydropower systems using an effective DE algorithm with mutation strategy adaptation (MSA-DE). Fang and Popole (2020) reported the improved multi-objective particle swarm algorithm (MOPSO) to maximize hydropower generation benefits and environmental protection.

Many studies have been reported on optimization of reservoir systems based on meta-heuristic algorithms under climate change (Azadi et al. 2021; Ashofteh et al. 2021; Golfam et al. 2021). Problem of hydropower optimization is a complex and non-linear problem. This work develops GOA and applies it to optimizing hydropower multi-reservoir operation, and compares performance of GOA with PSO, latter being a proven and successful method in optimizing water resources management (Jahandideh-Tehrani et al. 2020). Five operating modes are evaluated in this work, specifically two single-reservoir systems [Seymareh and Sazbon reservoir operated separately], two-reservoir systems [Seymareh reservoir and its upstream Sazbon reservoir, and Karkheh reservoir and its upstream Seymareh reservoir], and a three-reservoir system [Sazbon, Seymareh, Karkheh]. Reservoir operations are optimized under baseline (1976–2005) and two 30-year periods of climate change (2040–2069) and (2070–2099) subjected to greenhouse gases pathways RCP2.6, RCP4.5 and RCP8.5.

2 Methodology

First section presents three math test functions used to evaluate GOA. Second section presents simulation of future runoff with Artificial Neural Networks (ANNs). Third section presents a model of hydropower generation. Fourth section describes GOA, and fifth section briefly presents PSO, GOA and PSO results.

2.1 Mathematical Test Functions

The Ackley, Rastrigin, and Sphere function are used to evaluate GOA. Specifications of math test functions are listed in Table 1.

2.2 Runoff Simulation

An ANN is a special type of learning model that mimics certain functions of human brain. ANNs extract patterns embedded in data that are complex and difficult to identify with classic statistical methods.

2.3 Modeling of Hydropower Reservoir System

This work's objective function consists in minimizing shortage of hydropower-generated energy [Eq. (1)]:

$$Minimize\ DI = \frac{1}{T}\sum_{i=1}^{I}\sum_{t=1}^{T}\left(1 - \frac{E_{it}}{EGC_i}\right)^2 \tag{1}$$

where $E_{i,t}$ = energy generated by power plant of reservoir i in period t (GWh); EGC_i = energy generation capacity of power plant i (GWh); DI = deficit index, I and T denote number of reservoirs and periods of optimization, respectively.

Reservoir continuity equation is expressed by Eq. (2):

$$S_{i,t+1} = S_{i,t} + Q_{i,t} - RE_{i,t} - \frac{\left(A_{i,t} \times Eva_{i,t}\right)}{1000} - SP_{i,t} \tag{2}$$

where $S_{i,t+1}$ = storage of reservoir i at beginning of period $t+1$ (10^6 m^3); $S_{i,t}$ = storage of reservoir i at beginning of period t (10^6 m^3); $Q_{i,t}$ = river inflow to reservoir i during period t

Table 1 Mathematical test functions

Test function	Function	Search space	Global solution
Ackley	$20 + e - 20\exp(-0.2\sqrt{\frac{1}{D}(\sum_{d=1}^{D} x_d^2)})$	[− 32, 32]	0
Rastrigin	$10d + \sum_{d=1}^{D} [x_i^2 - 10\cos(2\pi x_i)]$	[− 5.12, 5.12]	0
Sphere	$\sum_{d=1}^{D} x_i^2$	[− 100, 100]	0

(10^6 m^3); $RE_{i,t}$ = water release reservoir i during period t (10^6 m^3); $A_{i,t}$ = lake surface area of reservoir i during period t (km^2); $Eva_{i,t}$ = evaporation from lake surface area of reservoir i in period t (mm), and $SP_{i,t}$ = spill volume of reservoir i during period t (10^6 m^3). Reservoir-spill constraint is defined by Eq. (3):

$$SP_{i,t+1} = \begin{cases} S_{i,t+1} - S_{\max,i} & if\ S_{i,t+1} > S_{\max,i} \\ 0 & else \end{cases} \tag{3}$$

where $S_{\max,i}$ = maximum storage volume of reservoir i (10^6 m^3).

Power generation, net water loss, and energy generation are calculated according to Eqs. (4) to (6), respectively:

$$P_{i,j} = \frac{RE_{ij} \cdot g \cdot e_i \cdot H_{netit}}{PF_i \cdot Mul \cdot 1000} \tag{4}$$

$$H_{neti,t} = ELV_{i,t} - TW_{i,t} \tag{5}$$

$$E_{i,t} = \frac{P_{i,t} \times PeakHour_i \times day}{1000} \tag{6}$$

where g = gravitational acceleration (m/s^2); e_i = efficiency of power plant i; $H_{neti,t}$ = net water loss of reservoir i during period t (meters); $P_{i,t}$ = power generated by plant i during period t (MW);PF$_\mathrm{i}$ PF_i = power plant performance factor of reservoir i; Mul = unit conversion factor; $ELV_{i,t}$ = water level of reservoir i during period t (meters above sea level); $TW_{i,t}$ = water level power plant i during period t (meters above sea level); day = number of days in a month; $PeakHour_i$ = peak hour for energy production of power plant i, and $E_{i,t}$ = energy generated by power plant of reservoir i during period t (GWh).

Constraints are applied to reservoir storage, release volume, and production capacity, which are expressed by Eqs. (7) through (9), respectively:

$$RE_{\min,i} \le RE_{i,t} \le RE_{\max,i} \tag{7}$$

$$S_{\min,i} \le S_{i,t} \le S_{\max,i} \tag{8}$$

$$0 \le P_{i,t} \le PPC_i \tag{9}$$

where $RE_{\min,i}$ = minimum release volume of reservoir i (10^6 m^3); $RE_{\max,i}$ = maximum release volume of reservoir i (10^6 m^3); $S_{\min,i}$ = minimum storage volume of reservoir i (10^6 m^3), and PPC_i = installed capacity of power plant i.

Penalty functions (PF_1 and PF_2) are added to (minimization) objective function to penalize violations of minimum storage constraint [Eqs. (10) and (11)]:

$$PF_1 = D \times (1 + S_{\min} - S_i)^2 \tag{10}$$

$$PF_2 = U \times \left(\frac{|S_{\min} - S_i|}{S_{\max} - S_{\min}} \right)^2 + Z \tag{11}$$

where D, U, Z = positive constant values (calculated by trial and error).

Surface-volume and water level-volume and functions of reservoirs are defined by Eqs. (12) and (13), respectively:

$$A_i = a_1 S_{i,t}^5 + b_1 S_{i,t}^4 + c_1 S_{i,t}^3 + d_1 S_{i,t}^2 + e_1 S_{i,t} + f_1 \tag{12}$$

$$H_i = a_2 S_{i,t}^5 + b_2 S_{i,t}^4 + c_2 S_{i,t}^3 + d_2 S_{i,t}^2 + e_2 S_{i,t} + f_2 \tag{13}$$

where H_i = level of reservoir i (meters above sea level); and parameters a_i, b_i, c_i, d, e_i, f_i = t coefficients corresponding to reservoir i.

Decision variable of problem is water released from reservoir. Since operating period is monthly for 30 years, number of decision variables equals 360. Also, optimization periods in this study include baseline and future periods (latter under RCP2.6, RCP4.5 and RCP8.5). Optimization solution is obtained by averaging results from three-run of GOA.

2.4 Grasshopper Optimization Algorithm (GOA)

GOA is a population-based meta-heuristic optimization method inspired by grasshopper group behavior (Saremi et al. 2017). Zeynali and Shahidi (2018) applied GOA to optimize coefficients of river suspended sediment rating equation. Khalifeh et al. (2020) used GOA to optimize nonlinear Muskingham flood-routing model. This work develops and applies GOA in field of hydropower generation. Grasshopper colonies have large populations. Position of grasshoppers is modeled according to Eq. (14):

$$X_{i'} = S_{i'} + G_{i'} + A_{i'} \tag{14}$$

where $X_{i'}$ = position of grasshopper i'; $S_{i'}$ = social interaction of grasshopper i'; $G_{i'}$ = Gravitational force applied to grasshopper i'; $A_{i'}$ = effect of wind force on grasshopper i'. Random behavior is introduced by rewriting Eq. (14) as Eq. (15):

$$X_{i'} = r_1 S_{i'} + r_2 G_{i'} + r_3 A_{i'} \tag{15}$$

where r_1, r_2, r_3 = random numbers between zero and one.

Social interaction derives from main concepts of grasshopper behavior and movement, as expressed by Eqs. (16) through (19):

$$S_{i'} = \sum_{\substack{j=1 \\ (i \neq j)}}^{N_P} s\left(d_{i'j'}\right)\hat{d}_{i'j'} \tag{16}$$

$$d_{i'j'} = \left|X_{j'} - X_{i'}\right| \tag{17}$$

$$\hat{d}_{i'j'} = \frac{X_{j'} - X_{i'}}{d_{i'j'}} \tag{18}$$

$$s = fe^{\frac{-r}{l}} - e^{-r} \tag{19}$$

where N_P = Number of grasshoppers; s = power of social forces; $d_{i'j'}$ = distance between grasshoppers i' and j'; $\widehat{d}_{i'j'}$ = distance vector between grasshoppers i' and j'; f = intensity of gravity; r = random number between zero and one; and l = gravity scale length.

Range of f is between zero and 1 and that of l is between 1 and 2. The s function divides space between two grasshoppers into areas of attraction force, comfort zone, and repulsion force. Force between two grasshoppers vanishes if distance separating them is large; therefore distance between any two grasshoppers is assumed between 1 and 4 (Sarmi et al. 2017). Gravitational ($G_{i'}G_{i'}$) and wind ($A_{i'}A_{i'}$) forces applied to grasshopper i are calculated according to Eqs. (20) and (21):

$$G_{i'} = -g\hat{e}_g \tag{20}$$

$$A_{i'} = u\hat{e}_w \tag{21}$$

where g = gravity constant; $\widehat{e}_g$ = unit vector oriented towards center of earth; u = constant thrust; and $\widehat{e}_w$ = unit vector along wind direction.

Substituting Eqs. (16) through (21) in Eq. (14) produces Eq. (22) expressing expanded position ($X_{i'}$) of particle i:

$$X_{i'} = \sum_{\substack{j'=1 \\ i'\neq j'}}^{N_p} s\left(\left|X_{j'} - X_{i'}\right|\right)\frac{X_{j'} - X_{i'}}{d_{i'j'}} - g\hat{e}_g + u\hat{e}_w \tag{22}$$

Equation (22) is suitable for modeling movement of grasshoppers in open space. Grasshopper or particle i's position ($X_{i'}^d$) used in optimization is given by Eq. (23):

$$X_{i'}^d = C\left\{\sum_{\substack{j' = 1 \\ i' \neq j'}}^{N_p} C\frac{ub_d - lb_d}{2}s\left|x_{j'} - x_{i'}\right|\frac{x_{j'} - x_{i'}}{d_{i'j'}}\right\} + \hat{T}_d \tag{23}$$

where ub_d = upper limit in d dimension; lb_d = lower limit in d dimension; $\hat{T}_d$ = position of the best solution found; and C = decrease coefficient.

The first C (before parentheses) in Eq. (23) strikes a balance between exploration and extraction, and second C (within parentheses) reduces attraction, comfort, and repulsion regions between grasshoppers. C is calculated by Eq. (24):

$$C = C_{\max} - t'\frac{C_{\max} - C_{\min}}{T'} \tag{24}$$

where $C_{\max}$ = maximum value of C (normally close to or equal to 1); $C_{\min}$ = minimum value of C (close to zero); T' = maximum number of algorithmic iterations. Flowchart of optimization algorithm is shown in Fig. 1.

2.5 Particles Swarm Optimization

PSO is inspired by social behavior of animals, including fish or birds living in small and large groups (Kennedy and Eberhart 1995). PSO introduces a number of variables called particles that are scattered in search space. Rules of self-organization in PSO

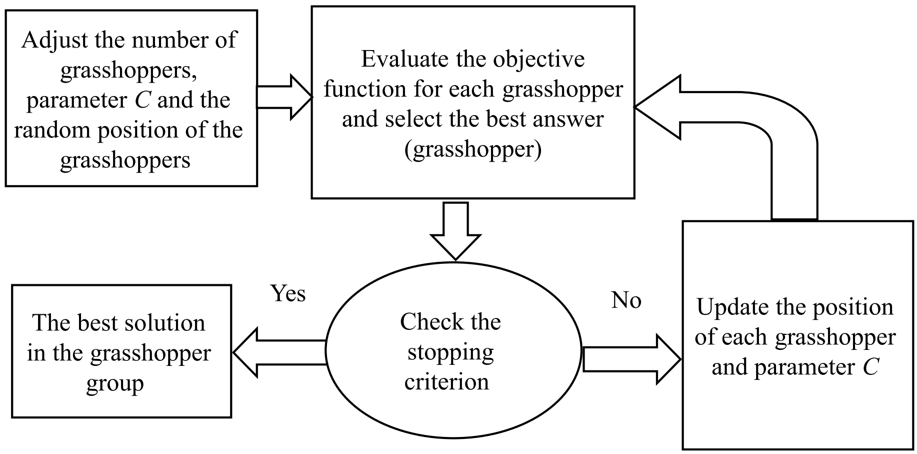

Fig. 1 GOA's flowchart

algorithmic iterations require that a particle must move some in direction of its current motion, some in direction of its best memory, and some in direction of the best memory of particle swarm to reach a new position. Particle *it's* new velocity vector (V_i^{t+1}) and position (X_i^{t+1}) are calculated from three vectors according to Eqs. (25) and (26):

$$V_i^{t+1} = \omega v_i^t + c_1 r_1 \left(X^{i,best} - X_j^t \right) + c_2 r_2 (X^{globalbest} - X_j^t) \tag{25}$$

$$X_i^{t+1} = X_i^t + V_i^{t+1} \tag{26}$$

where V_i^{t+1}=new particle velocity; ω=coefficient of inertia (whose optimal value is between 0.4 and 0.9, the lower the coefficient of inertia, the faster the algorithm converges); $X^{i,best}$=best position experienced by particle i; $X^{globalbest}$=best position experienced by swarm; c_1=personal learning factor; c_2=coefficient of collective learning; r_1, r_2 = vectors of position.

3 Study Area

This work assesses the operation of single-purpose hydropower reservoirs, namely, Sazbon, Seymareh and Karkheh reservoir in Iran. Seymareh reservoir is under operation, Sazbon and Karkheh reservoirs are in study phase. Power plants' installed capacity at Sazbon, Seymareh, and Karkheh equal 300, 480 and 360 MW, respectively.

Reason for choosing baseline (1976–2005) is that meteorological and hydrometric information and other items are available for this period. Fifth Intergovernmental Panel on Climate Change (IPCC) report includes historical data until 2005. In period 1976–2005 reservoirs were in their initial phase of operation.

Table 2 Optimal value of GOA and PSO parameters (for mathematical test functions and hydropower problem)

GOA (for mathematical test functions)					
Number of iterations	Number of populations	f	L	C_{max}	C_{min}
1000	50	0.5	1.3	1	10^{-6}
GOA (for hydropower problem)					
Number of iterations	Number of populations	f	L	C_{max}	C_{min}
1000	100	0.5–0.6	1.3–1.5	1	10^{-6}
PSO (for hydropower problem)					
Number of iterations	Number of population	W	φ_1, φ_2	C_1, C_2	
1000	100	0.6721–0.7298	2.05–2.08	1.3979–1.4962	

4 Results

4.1 GOA Evaluation Based on Mathematical Test Functions

Optimal values of parameters f, l, C_{min}, C_{max} and number of iterations for all three test functions are listed in Table 2. Optimal GOA parameters were calculated by trial and error. GOA values are listed in Table 3. GOA approached global minimum of Rastrigin function better than those of two other functions (see Fig. 2). Convergence curve of Ackley function has smaller concavity than other two functions. In fact, it exhibits faster convergence to optimal solution. In general, GOA exhibits accurate convergence rate to global optima of three test functions.

Table 3 Values of objective function (dimensionless) and run-time (in seconds) obtained from GOA for mathematical test functions

Run specifications	Mathematical test function					
	Ackley		Rastrigin		Sphere	
	Value	Time	Value	Time	Value	Time
Run I	8×10^{-6}	13.78	3×10^{-11}	13.7	2×10^{-10}	14.73
Run II	6×10^{-6}	13.85	4×10^{-11}	12.92	5×10^{-11}	13.37
Run III	7×10^{-5}	14.32	2×10^{-10}	13.56	4×10^{-10}	13.03
Best run	6×10^{-6}		3×10^{-11}		5×10^{-11}	
Worst run	7×10^{-5}		2×10^{-10}		4×10^{-10}	
Average runs	2×10^{-5}		9×10^{-11}		2×10^{-10}	
Standard deviation of runs	2×10^{-5}		9.5×10^{-11}		2×10^{-10}	
Best run time	13.78		12.9		13.03	

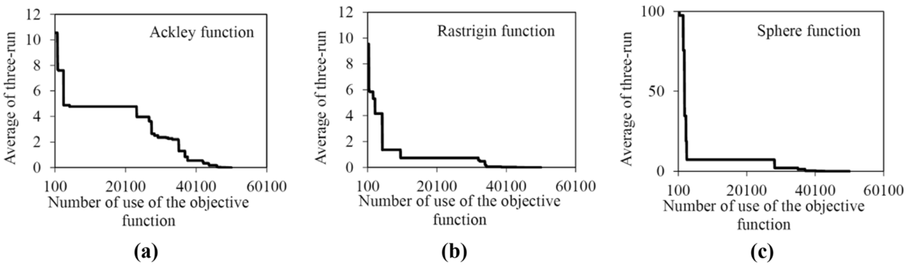

Fig. 2 Convergence diagram of mathematical test functions based on GOA for **a** Ackley, **b** Rastrigin, and **c** Sphere functions

4.2 Runoff Simulation Results

Time series of projected temperature was obtained from GFDL-ESM2M and projected rainfall was calculated with CNRM-CM5 for future. GFDL-ESM2M (with correlation coefficient equal to 99.3% and Root Mean Square Error (*RMSE*) equal to 2.1 °C) and CNRM-CM5 (with correlation coefficient equal to 87% and *RMSE* equal to 17.9 mm) had the best performances in simulating temperature and rainfall in baseline, respectively. ANN establishes a functional association between temperature, rainfall, and runoff in baseline, and simulates future runoff with future temperature and rainfall. ANNs with Nash–Sutcliffe efficiency (*NSE*) coefficient equal to 0.5 in training and test period for Seymareh and Karkheh rivers have the best performance with respect to runoff simulation. Simulated runoff in two rivers in future is displayed in Fig. 3.

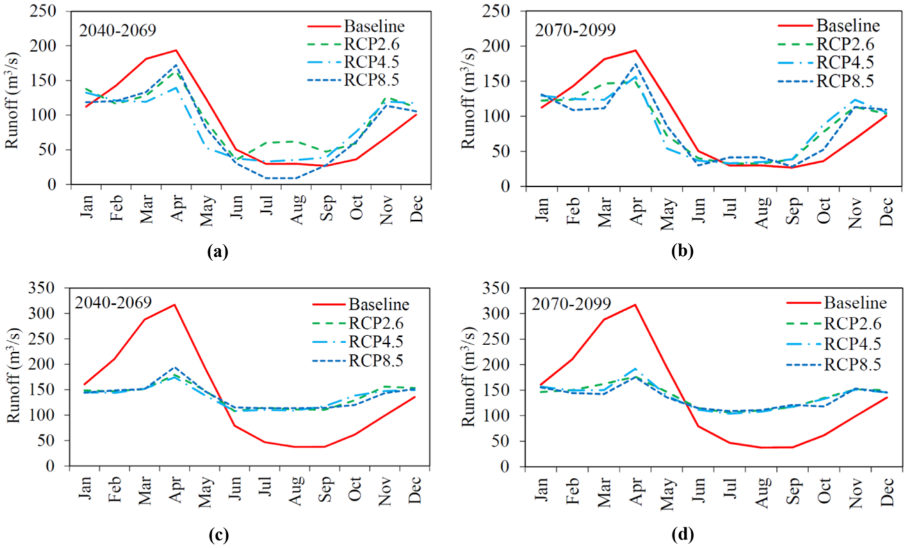

Fig. 3 Comparison of Seymareh river runoff in baseline, **a** 2040–2069, and **b** 2070–2099; and Karkheh River in baseline, **c** 2040–2069, and **d** 2070–2099

It is seen in Fig. 3a, b that Seymareh river's runoff in near future (2040–2069) under RCP2.6, RCP4.5 and RCP8.5 would increase by 3.9%, decrease by 6.5 and 10.2% compared to baseline, respectively; runoff in far future (2070–2099) would decrease by 4, 4.53, and 6% under RCP2.6, RCP4.5 and RCP8.5, respectively, compared to baseline. Comparison of long-term average monthly runoff in climate change with baseline reveals that peak flows would decrease in wet months, and would increase under some scenarios in relatively dry months. Also, long-term average monthly runoff for autumn shows an increase under climate change relative to baseline. According to Fig. 3c, d Karkheh River runoff in future would decrease under climate change compared to baseline. This rate of runoff reduction in 2070–2099 would be larger than in 2040–2069, so that long-term average monthly runoff in 2040–2069 under RCP2.6, RPC4.5, and RCP8.5 would decrease compared to baseline by 0.7, 2 and 0.7%, respectively, and in 2070–2099 it would decrease by 0.2, 0.6 and 2.6%, respectively. Rate of reduction of RCP8.5 in 2070–2099 is the largest compared to other climate change scenarios (2.6% reduction compared to baseline).

4.3 Results of Hydropower Optimization Obtained with GOA

In this work GOA parameters were optimized by trial and error for baseline and future. Parameter values in all periods and scenarios are listed in Table 2. Results of three-run of objective function and corresponding run-time for five operating modes are listed in Table 4. The best objective function obtained with first-mode of operation decreases in climate change compared to baseline. Minimum objective function in 2040–2069 is under RCP2.6 and maximum corresponds to baseline. Minimum run-time in 2070–2099 is under RCP8.5. Insofar as second-mode of operation is concerned minimum objective function in 2040–2069 is under RCP2.6 and maximum objective function corresponds to baseline. Minimum run-time in 2040–2069 is under RCP8.5. Objective function decreases in future compared to baseline. The best objective function calculated with third-mode of operation improves in future. Objective function in fourth-mode of operation decreases during climate change compared to baseline. Minimum objective function in 2040–2069 is under RCP4.5 and its maximum corresponds to baseline. In addition, minimum run-time of optimization corresponds to baseline. Objective function in fifth-mode of operation decreases in future compared to baseline.

Convergence diagram for five operating modes is displayed in Fig. 4. Reservoir system in first-mode of operation in 2040–2069 under RCP2.6 exhibits a better performance in achieving optimal objective function than under RCP4.5 and RCP8.5. Also, system in 2070–2099 under RCP2.6 would perform better than other two scenarios in achieving optimal objective function. GOA performed better in second-mode of operation and 2040–2069 under RCP2.6 in achieving desired objective function. The best performance of GOA in achieving optimal objective function in 2070–2099 compared to baseline is under RCP2.6. GOA performed better in third-mode of operation and 2040–2069 under RCP2.6 to achieve optimal objective function. Convergence diagrams for future show less concavity than in baseline, and under RCP8.5 it performs better in reaching solution. GOA's performance with fourth-mode of operation in 2040–2069 under RCP2.6 was better than RCP4.5 and RCP8.5. GOA calculated the lowest objective function in fourth-mode of operation for 2070–2099 under RCP2.6. In fifth-mode of operation GOA had better performance in achieving optimal objective function in future than baseline, and in 2070–2099 it calculated the best objective function.

Table 4 Objective function values (dimensionless) and run-time (in seconds) obtained from GOA in first to fifth-mode of operation in baseline and future

Run specifications	Baseline		2040–2069						2070–2099					
			RCP2.6		RCP4.5		RCP8.5		RCP2.6		RCP4.5		RCP8.5	
	Value	Time	Value	Time	Value	Time	Value	Time	Value	Time	Value	Time	Value	Time
First-mode of operation														
Run I	17.4	212.3	5×10^{-6}	210	0.01	209	0.01	220	6×10^{-8}	211	0.01	215	0.01	210
Run II	15.6	220	10^{-7}	218	0.01	214	0.01	217	5×10^{-8}	216	0.02	216	0.01	230
Run III	14.6	216	8×10^{-8}	214	0.01	217	0.01	220	3×10^{-8}	213	0.01	218	0.01	209
Best run	14.6		8×10^{-8}		0.01		0.01		5×10^{-8}		0.01		0.01	
Worst run	17.4		5×10^{-6}		0.01		0.01		0.0000203		0.01		0.01	
Average runs	15.9		2×10^{-6}		0.01		0.01		6×10^{-6}		0.01		0.01	
Standard deviation of runs	1.4		3×10^{-6}		0.0006		0.0008		1.2×10^{-5}		0.003		0.0002	
Best run time	212.3		210		209		217		211		215		209	
Second-mode of operation														
Run I	81.1	238	0.2	217.7	9.4	212.86	57.7	213.32	12.1	227.5	9.2	217	25.9	218.2
Run II	86.6	224	0.3	216.9	10.8	214.55	60.9	210.2	11.9	221.4	8.7	216.3	21.3	219
Run III	87.4	243	0.3	214.8	10.1	212.25	61	208.8	11.5	215.5	11.4	221.4	23.1	221.1
Best run	81.1		0.2		9.4	57.7	11.5	8.7	21.3	Best run	81.1		0.2	
Worst run	87.4		0.3		10.8	61	12.1	11.4	25.9	Worst run	87.4		0.3	
Average runs	85		0.3		10.10	59.9	11.8	9.8	23.4	Average runs	85		0.3	
Standard deviation of runs	3.4		0.1		0.7	1.9	0.3	1.5	2.3	Standard deviation of runs	3.4		0.1	
Best run time	224		214.8		212.2	208.8	215.5	216.3	218.2	Best run time	224		214.8	
Third-mode of operation														
Run I	101.1	448	0.4	448.6	29.3	454.9	57.4	446.3	13.6	461	10.9	445.2	11.4	447.7
Run II	104.2	443.7	0.2	453.2	27.7	453	55	443.7	16.3	446.2	17	445.5	10.2	446
Run III	95.8	443.8	0.4	526	21.2	537.8	54.3	442.7	14.8	449.2	12.8	446.8	11.2	480.3
Best run	95.8		0.2		21.2		54.3		13.6		10.9		10.9	
Worst run	104.2		0.4		29.3		57.4		16.3		17		11.9	

Table 4 (continued)

Run specifications	Baseline		2040–2069						2070–2099					
			RCP2.6		RCP4.5		RCP8.5		RCP2.6		RCP4.5		RCP8.5	
	Value	Time	Value	Time	Value	Time	Value	Time	Value	Time	Value	Time	Value	Time
Average runs	100.4		0.3		26		55.6		14.9		13.6		0.6	
Standard deviation of runs	4.2		0.1		4.3		1.6		1.4		3.1		0.6	
Best run time	443.7		448.6		453		442.7		446.2		445.2		446	
Fourth-mode of operation														
Run I	40.9	456.9	1.8	457.8	0.01	453	3	501	1	454.7	1	470.2	1	499.8
Run II	42.6	451.8	2.7	461.7	5.4	455.9	4.6	457	1	479	1	454.3	2.4	465
Run III	38.3	469	3.9	464.7	3.3	497.4	3.1	478.4	1	477.8	1.2	463.9	1	494.8
Best run	38.3		1.8		0.01		3		1		1		1	
Worst run	42.6		3.9		5.4		4.6		1		1.2		2.4	
Average runs	40.6		2.8		2.9		3.6		1		1		1.5	
Standard deviation of runs	2.2		1		2.7		0.9		0.8		0.1		0.8	
Best run time	451.8		457.8		453		457		454.7		454.3		465	
Fifth-mode of operation														
Run I	20.4	647.6	3.9	684.8	10	631.2	9.2	647.4	5.3	654.8	1	632.2	2	648.4
Run II	17.5	647.9	7.3	681.3	7.3	640.6	10.8	655.4	6.3	660.4	3	643.3	1.5	658.3
Run III	26.7	644.2	8.5	679.7	8.5	650.7	9.1	651.6	6.4	667.4	1	659.1	2.9	656.8
Best run	17.5		2.4		7.2		9.1		5.3		1		1.5	
Worst run	26.77		3.9		10		10.8		6.4		3		2.9	
Average runs	21.5		3.1		8.6		9.7		6		1.7		2.1	
Standard deviation of runs	4.7		0.7		1.4		0.9		0.6		1.1		0.7	
Best run time	644.2		679.7		631.2		647.4		654.8		632.2		648.4	

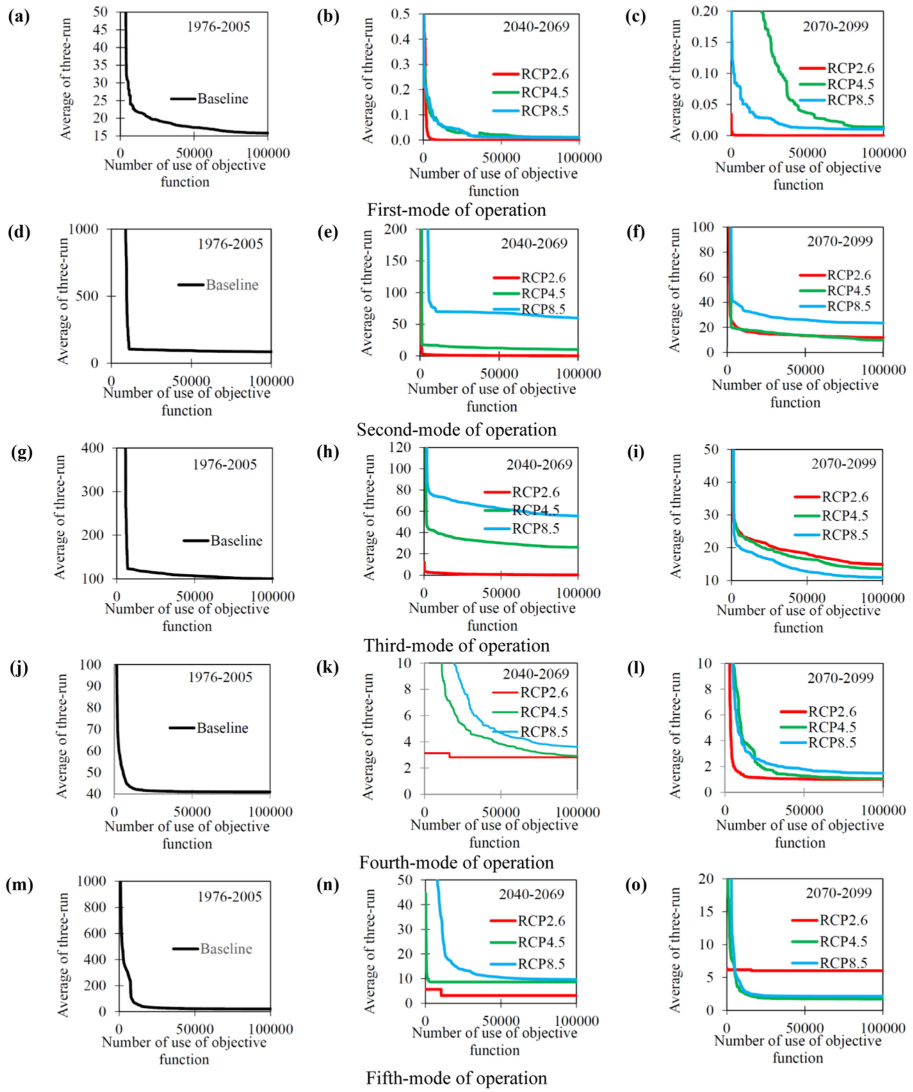

Fig. 4 Convergence diagram of average of three-run of GOA for first-mode in **a** baseline, **b** 2040–2069, **c** 2070–2099; with second-mode in **d** baseline, **e** 2040–2069, **f** 2070–2099; with third-mode in **g** baseline, **h** 2040–2069, **i** 2070–2099; with fourth-mode in **j** baseline, **k** 2040–2069, **l** 2070–2099; with fifth-mode in **m** baseline, **n** 2040–2069, **o** 2070–2099

Calculated generated energy (average energy obtained from three-run) for five operating modes is depicted in Fig. 5. For first-mode of operation energy production of Sazban power plant would increase in future compared to baseline, that is, it would generate entire energy production capacity. Long-term production energy of power plant in baseline increases by 8.8% compared to future. Insofar as second-mode of operation is concerned energy produced in future would increase compared to baseline. Maximum energy production in 2040–2069 would be under RCP2.6. Maximum energy production in 2070–2099 is under RCP2.6 and

Fig. 5 Comparison of monthly long-term generation energy in baseline by GOA in first-mode of operation ▶ in **a** 2040–2069 and **b** 2070–2099; with second-mode in **c** 2040–2069 and **d** 2070–2099; with third-mode in **e** 2040–2069 and **f** 2070–2099; with fourth-mode in **g** 2040–2069 and **h** 2070–2099; with fifth-mode in **i** 2040–2069 and **j** 2070–2099

RCP4.5. Energy produced with third-mode of operation in future would increase compared to baseline, and rate of increase in 2070–2099 would be larger than in 2040–2069. Rate of increase in energy generation in 2040–2069 under RCP2.6 would be higher. Increase in energy for 2070–2099 would approximately the same under all three-scenario. Approximately total energy generation capacity would be generated in 2040–2069 under RCP2.6. Long-term energy generated in 2040–2069 under RCP2.6 with fourth-mode of operation would provide total energy capacity. Energy generation capacity in 2070–2099 with fourth-mode of operation under RCP2.6 and RCP4.5 would be achieved. Minimum energy produced under RCP8.5 would be in 2040–2069. Concerning fifth-mode of operation energy production would increase in future. Total energy generation capacity would be provided under RCP2.6 and RCP4.5 with fifth-mode of operation. In general, more energy would be generated in 2070–2099 than in 2040–2069.

Results of reservoir storage and release based calculated with GOA in climate change compared to those for baseline are listed in Table 5 as minimum, average, and maximum corresponding to five operating modes. Reservoir storage volume would increase in future compared to baseline, and rate of increase in 2070–2099 would be greater than in 2040–2069. Release from reservoir in future shows an increase compared to baseline. Rate of increase in release in 2040–2069 would be higher than in 2070–2099.

4.4 Results of PSO Based Optimization

Performance of GOA in optimizing hydropower generation was compared with hydropower optimization based on PSO. Optimized PSO parameters are listed in Table 2.

Results of three-run and their run-times for five operating modes are listed in Table 6. In first-mode of operation minimum objective function in 2070–2099 corresponds to RCP4.5, and its maximum in baseline equals 0.6. The best objective function obtained with second-mode of operation in future is reduced compared to baseline, and minimum objective function in 2040–2069 is under RCP2.6, and in 2070–2099 it is under RCP4.5. Minimum run-time of objective function corresponds to baseline. The best objective function calculated with third-mode of operation decreases in future compared to baseline, and reduction would be higher in 2040–2069 under RCP2.6. Minimum run-time in 2070–2099 is under RCP2.6. Minimum objective function obtained with fourth-mode of operation in 2070–2099 is under RCP4.5, and its maximum corresponds to baseline. In general, objective function in future shows a significant decrease compared to baseline. Minimum objective function with fifth-mode of operation in 2070–2099 is under RCP2.6, and its maximum corresponds to baseline.

Convergence diagrams for five modes of operating obtained with PSO are depicted in Fig. 6. For first-mode of operation PSO converge faster in future than baseline. Maximum objective function has an average value of 0.6 in baseline. PSO exhibited a good performance in calculating the best objective function with second-mode of operation, in future compared to baseline. In general, performance of PSO in future is better than baseline. The best objective function in this mode of operation based on PSO in 2040–2069 is under RCP2.6. The best performance of PSO with third-mode of operation under RCP2.6 is in

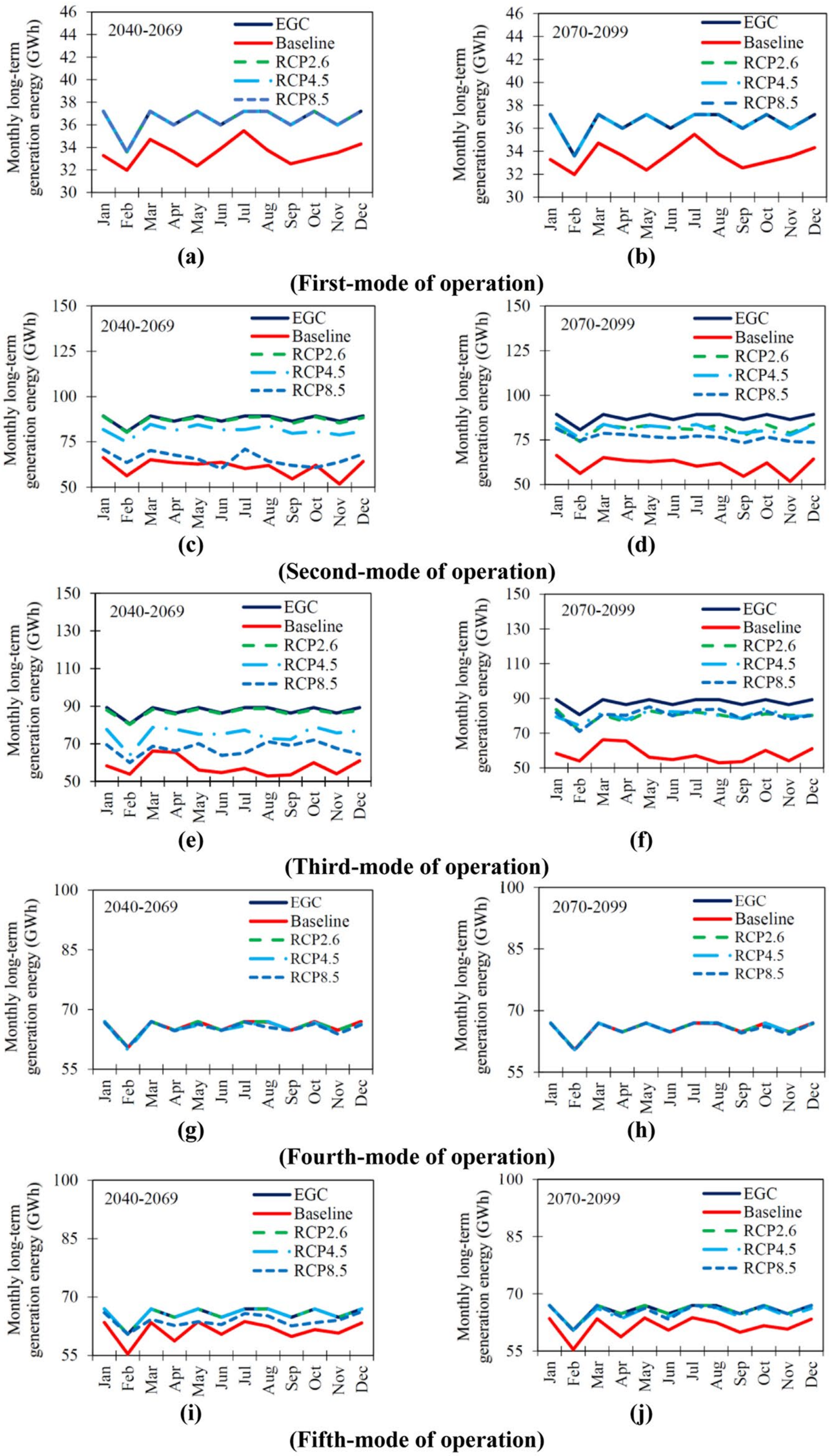
Monthly long-term generation energy (GWh)
2040-2069
2070-2099
EGC
Baseline
RCP2.6
RCP4.5
RCP8.5
Jan Feb Mar Apr May Jun Jul Aug Sep Oct Nov Dec
(a)
(b)
(First-mode of operation)
(c)
(d)
(Second-mode of operation)
(e)
(f)
(Third-mode of operation)
(g)
(h)
(Fourth-mode of operation)
(i)
(j)
(Fifth-mode of operation)

Table 5 Minimum, average and maximum reservoir storage and release (10^6 m^3) in baseline and future for different operating modes based on GOA

Mode	Characteristic	Scenario	1976–2005			2040–2069			2070–2099		
			Min	Ave	Max	Min	Ave	Max	Min	Ave	Max
First	Storage volume	RCP2.6	926	1377	1576	1092	1481	1575	1025	1441	1575
		RCP4.5				937	1406	1575	1090	1428	1575
		RCP8.5				942	1351	1575	1023	1422	1575
	Release	RCP2.6	45	141	287	108	170	269	126	168	182
		RCP4.5				122	168	230	121	170	225
		RCP8.5				130	168	207	126	168	225
Second	Storage volume	RCP2.6	1669	2153	2474	1665	2156	2473	1663	2083	2473
		RCP4.5				1665	2101	2473	1663	2097	2473
		RCP8.5				1664	2112	2473	1663	2112	2473
	Release	RCP2.6	1	188	444	165	226	294	86	213	328
		RCP4.5				119	211	238	70	211	332
		RCP8.5				89	191	408	42	208	333
Third	Storage volume	RCP2.6	1767	2179	2473	1689	2181	2473	1682	2102.9	2473
		RCP4.5				1678	2111	2473	1680	2106	2473
		RCP8.5				1683	2117	2473	1738	2078	2473
	Release	RCP2.6	4	194	438	158.6	225.2	312.7	78	212.5	352
		RCP4.5				47	203	383	97	211	340
		RCP8.5				14	195	369	99	209	336
Fourth	Storage volume	RCP2.6	93	128	131	107	104	131	106	129	131
		RCP4.5				94	128	131	97	129	131
		RCP8.5				94	128	131	106	129	131
	Release	RCP2.6	16	148	252	47	154	264	54	151	242
		RCP4.5				10	147	272	69	152	246
		RCP8.5				36	145	271	51	152	255
Fifth	Storage volume	RCP2.6	92	127	131	108	130	131	108	130	131
		RCP4.5				93	128	131	105	129	131
		RCP8.5				92.5	128	131	101	129	131
	Release	RCP2.6	100	127	260	108	150	305	108	130	301
		RCP4.5				23	147	255	105	129	295
		RCP8.5				92	128	200	101	129	305

2040–2069, and PSO calculated much lower initial objective function. In general, PSO performs better in future than baseline for achieving optimal objective function. Maximum objective function is in baseline. Convergence rate with fourth-mode of operation obtained with PSO is high in baseline and future. PSO converges rapidly with fifth-mode of operation in baseline and future, and objective function in 2040–2069 and 2070–2099 under RCP2.6 is close to best value compared to other climate change scenarios.

Energy generation for five modes of operation and energy generation capacity of power plant are depicted in Fig. 7. In first-mode of operation energy produced by Sazbon power plant in future would increase compared to baseline and rate of increase in 2070–2099 would be larger than in 2040–2069. Minimum energy production with second-mode of operation, at Seymareh power plant in 2040–2069 is under RCP8.5 and maximum is under

Table 6 Objective function values (dimensionless) and run-time (in seconds) obtained from PSO with first to fifth-mode of operation in baseline and future

Run specifications	Baseline		2040–2069						2070–2099					
			RCP2.6		RCP4.5		RCP8.5		RCP2.6		RCP4.5		RCP8.5	
	Value	Time	Value	Time	Value	Time	Value	Time	Value	Time	Value	Time	Value	Time
First-mode of operation														
Run I	0.5	134	0.003	140	0.3	135	0.02	135	0.03	136	0.002	136	0.02	134
Run II	0.6	134	0.02	136	0.07	136	0.01	134	0.001	136	0.001	136	0.007	135
Run III	0.7	135	0.01	136	0.2	137	0.04	135	0.001	137	0.02	135	0.007	134
Best run	0.5		0.003		0.07		0.01		0.001		0.001		0.007	
Worst run	0.7		0.01		0.2		0.04		0.03		0.02		0.02	
Average runs	0.6		0.01		0.16		0.02		0.01		0.007		0.01	
Standard deviation of runs	0.1		0.0008		0.0007		0.001		0.001		0.001		0.0007	
Best run time	134		136		135		134		136		135		134	
Second-mode of operation														
Run I	10	135	0.01	136.3	1.3	137.7	3.7	137.8	0.5	138.7	0.01	136.1	1.1	135.5
Run II	11.3	134	0.02	135.7	2.2	137.6	4.2	136.1	0.3	135.1	0.03	135.6	0.5	136.9
Run III	11.6	135	0.01	134.9	2.9	135.5	6	136.9	0.2	134.2	0.4	135.8	0.6	134.1
Best run	10		0.01		1.3		3.7		0.2		0.01		0.5	
Worst run	11.6		0.02		2.9		6		0.5		0.4		1.1	
Average runs	10.9		0.1		2.15		4.9		0.3		0.1		0.8	
Standard deviation of runs	0.8		0.01		0.8		1.6		0.1		0.2		0.3	
Best run time	134		134.9		135.5		136.1		134.2		135.6		134.1	
Third-mode of operation														
Run I	17.6	280.7	2.7×10^{-6}	280.9	2.1	278.8	1.3	281.7	6.9	281.7	1.5	281.2	1	288.7
Run II	17.1	288.5	0.01	281.3	1.8	278.4	0.9	283.4	12.2	284.9	1.5	295.3	1.3	287.7
Run III	20.5	284.2	0.01	280.8	2.1	279.5	0.6	288.6	16.9	279.3	1.6	291.8	1.3	289.4
Best run	17.1		2.7×10^{-6}		1.8		0.6		6.9		1.5		1	
Worst run	20.5		0.01		2.1		1.3		16.9		1.6		1.3	

Table 6 (continued)

Run specifications	Baseline		2040–2069						2070–2099					
			RCP2.6		RCP4.5		RCP8.5		RCP2.6		RCP4.5		RCP8.5	
	Value	Time	Value	Time	Value	Time	Value	Time	Value	Time	Value	Time	Value	Time
Average runs	18.4		0.007		2.02		0.9		12		1.5		1.2	
Standard deviation of runs	1.8		0.006		0.2		0.2		5		0.05		0.2	
Best run time	280.7		280.9		287.4		281.7		280.3		281.2		287.7	
Fourth-mode of operation														
Run I	1	279	0.008	272	0.007	279	0.002	278	0.05	279	0.008	277.9	0.001	278.3
Run II	1	277	0.0004	290	0.06	278	0.06	277	0.01	279	0.02	278.5	0.05	277.4
Run III	1	290	0.001	279	0.01	277	0.01	278	0.02	277	3×10^{-5}	277.2	0.006	277.5
Best run	1		0.003		0.007		0.002		0.001		3×10^{-5}		0.001	
Worst run	1		0.004		0.06		0.006		0.005		0.02		0.05	
Average runs	1		0.003		0.02		0.02		0.03		0.009		0.02	
Standard deviation of runs	0		0.004		0.003		0.003		0.02		0.01		0.03	
Best run time	277		270.7		277.2		277.5		276.6		277.9		277.3	
Fifth-mode of operation														
Run I	1	402.2	9×10^{-5}	420	0.0001	407.06	0.04	407.9	0.0009	423	0.05	410	0.06	405.8
Run II	1	403.6	2×10^{-5}	409.8	0.01	412.7	0.01	406.1	6×10^{-5}	419.8	0.02	413.7	0.02	406.2
Run III	1	404.9	2×10^{-5}	410.3	0.0008	406.2	0.001	402.9	8×10^{-7}	418.3	0.007	416.2	0.01	404.6
Best run	1		2×10^{-5}		0.0001		0.001		8×10^{-7}		0.007		0.01	
Worst run	1		9×10^{-5}		0.01		0.01		6×10^{-5}		0.05		0.06	
Average runs	1		4×10^{-5}		0.004		0.017		4.3×10^{-5}		0.03		0.03	
Standard deviation of runs	0		4×10^{-5}		0.005		0.02		4×10^{-5}		0.02		0.02	
Best run time	402.2		409.8		406.2		402.9		418.3		410		404.6	

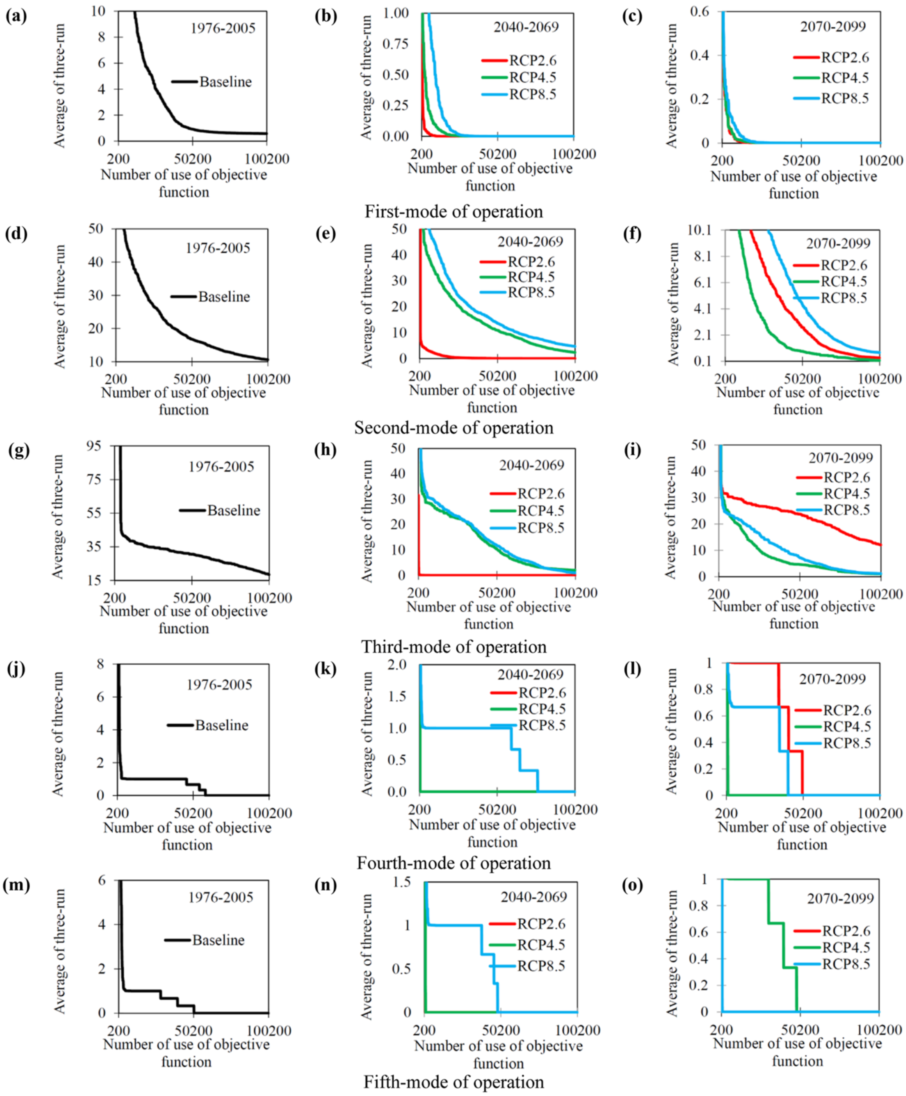

Fig. 6 Convergence diagram of average of three-run of PSO with first-mode in **a** baseline, **b** 2040–2069, **c** 2070–2099; with second-mode in **d** baseline, **e** 2040–2069, **f** 2070–2099; with third-mode in **g** baseline, **h** 2040–2069, **i** 2070–2099; with fourth-mode in **j** baseline, **k** 2040–2069, **l** 2070–2099; with fifth-mode in of **m** baseline, **n** 2040–2069, **o** 2070–2099

RCP2.6. Energy produced by Seymareh power plant would increase in 2070–2099 compared to baseline. Increase in energy production in 2070–2099 would be larger than in 2040–2069. Under RCP2.6 in 2040–2069 entire energy production capacity would be provided. Energy produced with third-mode of operation during future would increase compared to baseline, and this increase in energy generation would be larger in 2040–209 than 2070–2099. Maximum energy production in 2040–2069 is under RCP2.6 and minimum in 2070–2099 is under RCP8.5. Under RCP2.6 in 2040–2069 entire energy production

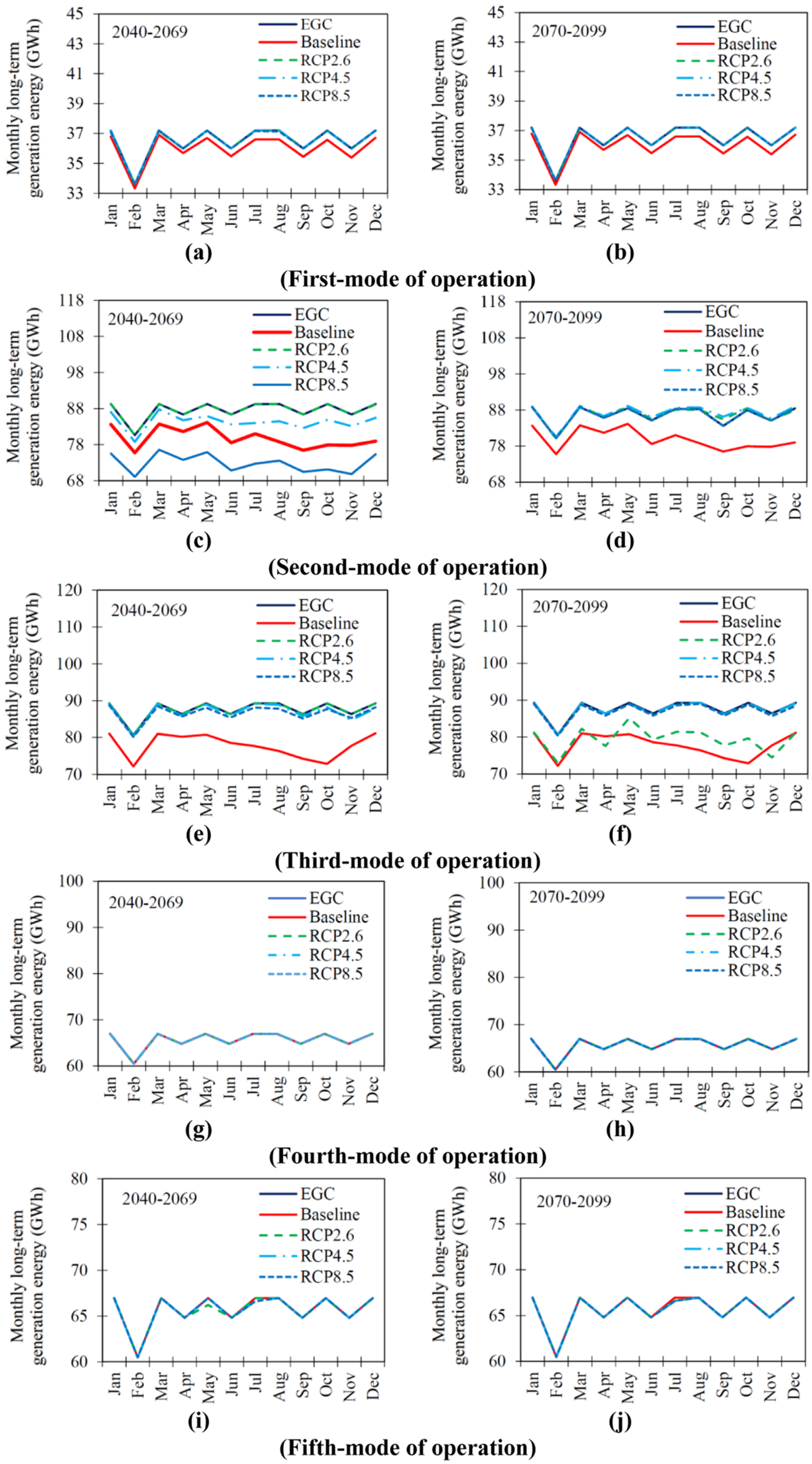
Monthly long-term generation energy (GWh)
2040-2069
2070-2099
EGC
Baseline
RCP2.6
RCP4.5
RCP8.5
Jan Feb Mar Apr May Jun Jul Aug Sep Oct Nov Dec
(a)
(b)
(First-mode of operation)
(c)
(d)
(Second-mode of operation)
(e)
(f)
(Third-mode of operation)
(g)
(h)
(Fourth-mode of operation)
(i)
(j)
(Fifth-mode of operation)

◀ **Fig. 7** Comparison of monthly long-term generation energy in baseline from PSO with first-mode of operation in **a** 2040–2069 and **b** 2070–2099; with second-mode in **c** 2040–2069 and **d** 2070–2099; with third-mode in **e** 2040–2069 and **f** 2070–2099; with fourth-mode in **g** 2040–2069 and **h** 2070–2099; with fifth-mode in **i** 2040–2069 and **j** 2070–2099

capacity would be provided. Energy production obtained with fourth-mode of operation at Karkheh power plant would equal to energy capacity in baseline and future. Energy production at Karkheh power plant with fifth-mode of operation in 2040–2069 under RCP2.6 would decrease by 0.09% compared to baseline. Reduction of energy production in 2070–2099 compared to baseline with respect to three scenario would be equal to 0.04%, and this reduction would occur in July.

Table 7 Minimum, average and maximum volume of reservoir storage and release (10^6 m^3) in baseline and future for different operating modes based on PSO

Mode	Characteristic	Scenario	1976–2005			2040–2069			2070–2099		
			Min	Ave	Max	Min	Ave	Max	Min	Ave	Max
First	Storage volume	RCP2.6	920	1357	1575	1067	1480	1575	1074	1437	1575
		RCP4.5				964	1407	1575	1070	1436	1575
		RCP8.5				935	1359	1575	1029	1426	1575
	Release	RCP2.6	91	174	288	127	171	237	121	168	220
		RCP4.5				113	167	243	112	169	229
		RCP8.5				117	167	226	120	167	223
Second	Storage volume	RCP2.6	1673	2127	2473	1762	2175	2473	1702	2173	2473
		RCP4.5				1677	2135	2473	1720	2169	2473
		RCP8.5				1700	2086	2473	1728	2134	2473
	Release	RCP2.6	75	208	375	167	231	359	147	215	331
		RCP4.5				105	209	383	118	209	372
		RCP8.5				80	201	366	84	213	354
Third	Storage volume	RCP2.6	1703	2160	2473	1079	2275	2473	1617	2130	2473
		RCP4.5				1873	2234	2473	1752	2229	2473
		RCP8.5				1788	2188	2473	1844	2182	2473
	Release	RCP2.6	62	190	386	129	127	343.5	102	211	365
		RCP4.5				101	201	372	123	207	371
		RCP8.5				112	198	372	122	205	342
Fourth	Storage volume	RCP2.6	104	129	131	113	131	131	113	130	131
		RCP4.5				107	130	131	106	130	131
		RCP8.5				105	130	131	112	130	131
	Release	RCP2.6	65	148	256	95	154	232	102	153	216
		RCP4.5				93	152	206	94	152	229
		RCP8.5				91	151	218	103	153	209
Fifth	Storage volume	RCP2.6	107	130	131	97	128	131	123	131	131
		RCP4.5				103	129	131	103	130	131
		RCP8.5				99	129	131	99	129	131
	Release	RCP2.6	65	151	228	46	148	249	75	157	222
		RCP4.5				74	151	212	88	152	225
		RCP8.5				60	149	239	44	143	264

Reservoir storage and release in future compared to baseline are listed as minimum, average, and maximum for five operating modes calculated with PSO are listed in Table 7. First-mode of operation produces a decreases of reservoir release in future compared to baseline, and this reduction would be larger in 2070–2099 than 2040–2069. Reservoir storage under climate change would increase compared to baseline. Reservoir releases increase significantly with second-mode of operation. Increase in reservoir release in 2040–2069 under RCP2.6 would be greater than in baseline. Reservoir storage increases significantly under climate change compared to baseline. Reservoir storage with third-mode of operation in future would increase significantly compared to baseline. Maximum reservoir storage in 2040–2069 is under RCP4.5. Reservoir releases would increase during future compared to baseline, and this increase would be greater in 2070–2099 than 2040–2069. Reservoir storage increases during future compared to baseline with fourth-mode of operation. Reservoir storage would increase in 2040–2069 under RCP2.6, RCP4.5 and RCP8.5 by 1.3, 0.5, and 0.6%, respectively. Reservoir releases increase during future compared to baseline, and this increase is greater in 2070–2099 than 2040–2069. Reservoir storage with fifth-mode of operation in future would increase significantly compared to baseline. This increase would be larger in 2070–2099 than 2040–2069. Reservoir releases would increase during future compared to baseline, and this increase would be greater in 2070–2099 than 2040–2069.

5 Concluding Remarks

GOA was applied to optimize multi-reservoir hydropower system. Optimization was performed for Sazbon, Seymareh and Karkheh reservoirs Iran. Objective function was to minimize hydropower energy shortage. Objective function based on GOA was implemented for five operating modes in baseline and future. Objective function in climate change calculated with first-mode of operation shows a significant decrease compared to baseline. Minimum objective function in 2040–2069 is under RCP2.6. Sazbon power plant produces entire energy production capacity. Optimization for second-mode of operation based on GOA showed that maximum objective function in baseline and minimum objective function in 2040–2069 are under RCP2.6. Objective function with third-mode of operation in future would decline compared to baseline, and its minimum in 2040–2069 is under RCP2.6. The best objective function with fourth-mode of operation in 2040–2069 is under RCP4.5, and maximum objective function corresponds to baseline. Power plant provides entire energy production capacity with fourth-mode of operation. Minimum objective function with fifth-mode of operation in future is under RCP4.5, and its maximum is in baseline. In general, GOA produces more energy in future than in baseline.

Increase in energy production and consequently decrease in deficit of energy supply in climate change context compared to baseline are due to change in runoff. Reducing peak flows in wet months, mainly in February to June, reduces reservoir spill and increases reservoir storage, and reservoir releases would increase to meet hydropower requirements, and, thus, shortages during future would decrease compared to baseline. For example, in second-mode of operating, Minimum energy production in baseline would be in September and November, and maximum percentage of changes in energy production in future compared to baseline in corresponding months (i.e., maximum percentage of changes in energy production compared to baseline in 2040–2069 under RCP2.6) would will increase by 65 and 55% in September and November, respectively.

PSO results for first-mode of operation showed that energy produced by power plant increases in future compared to baseline. Objective function in baseline equals 0.6. Objective function calculated with second-mode of operation decreases in future compared to baseline. Minimum objective function in 2040–2069 is under RCP2.6 and maximum corresponds to baseline. Minimum objective function obtained with third-mode of operation in 2040–2069 is under RCP2.6, in 2070–2099 is under RCP4.5, and its maximum corresponds to baseline. PSO optimizes energy production to its installed capacity in fourth and fifth-modes of operation.

The better performance of PSO than GOA in achieving optimal objective function is due to differences in structure of algorithms. GOA's C parameter C (which balances exploration and exploitation) depends on number of iterations, and because of this dependence, it seems that at beginning of optimization equilibrium between exploration and exploitation does not occur. On the other hand, equivalent parameter ω in PSO is independent of iterations and optimizes well in modified algorithmic version.

In general, PSO has shorter run-time than GOA in achieving the best objective function, however GOA has better performance and more stable solutions. This paper results indicate that if current version of GOA is modified it has potential to perform close to or even better than PSO in terms of run-time. Previous works have shown that algorithmic improvement can lead to increased computational accuracy, reduced run-time, and improved convergence. For example, Garousi-Nejad et al. (2016a) reported the Modified Firefly Algorithm (MFA). MFA results were compared with other optimization methods. MFA results proved superior solving test problems and exhibited potential for exploiting multi-reservoir problems over other methods. Xu and Mei (2018) proposed a modified Water Cycle Algorithm (WCA) based on diversity evaluation and Chaos theory (DC-WCA). Six mathematical test functions were examined to evaluate DC-WCA. The latter authors also applied four algorithms to optimize multi-reservoir hydropower systems. Their results suggest that DC-WCA has higher computational accuracy, shorter run-time, and faster convergence than other methods. Feng et al. (2020) proposed Quasi-opposition Sine Cosine Algorithm (QSCA). They compared proposed method with several well-known evolutionary methods. Their results indicate that convergence speed and quality of QSCA solution was better than those of other methods. Therefore, it seems that further studies on GOA could lead to better results by modifying parameter C (i.e., creating a balance between exploration and exploitation as well as reducing gravitational, neutral, and repulsion areas of grasshoppers).

Author Contributions KR developed theory and performed computations. P-SA verified analytical methods and encouraged KR to investigate specific aspects. P-SA supervised findings of this work, and HL helped supervise project. All authors discussed results and contributed to final manuscript. KR wrote manuscript with support from P-SA, and especially HL. P-SA conceived original idea.

Funding Not applicable.

Availability of Data and Materials Authors have restrictions on sharing data.

Declarations

Conflict of interest All authors declare that they have no conflict of interest.

References

Ahmadianfar I, Samadi-Koucheksaraee A, Bozorg-Haddad O (2017) Extracting optimal policies of hydropower multi-reservoir systems utilizing enhanced differential evolution algorithm. Water Resour Manag 31(14):4375–4397

Ahmadianfar I, Bozorg-Haddad O, Chu X (2019) Optimizing multiple linear rules for multi-reservoir hydropower systems using an optimization method with an adaptation strategy. Water Resour Manag 33:4265–4286

Ashofteh P-S, Bozorg-Haddad O, Loáiciga HA (2021) Application of bi-objective genetic programming (BO-GP) for optimizing irrigation rules using two reservoir performance criteria. Int J River Basin Manag. https://doi.org/10.1080/15715124.2019.1613415

Azadi F, Ashofteh P-S, Shokri A, Loáiciga HA (2021) Simulation-optimization of reservoir water quality under climate change. J Water Resour Plan Manag 147(9):04021054

Bozorg-Haddad O, Hosseini-Moghari SM, Loáiciga HA (2016) Biogeography-based optimization algorithm for optimal operation of reservoir systems. J Water Resour Plan Manag 142(1):04015034

Bozorg-Haddad O, Garousi-Nejad I, Loaiciga HA (2017) Extended multi-objective firefly algorithm for hydropower energy generation. J Hydroinform 19(5):734–751

Chang J, Wang X, Li Y, Wang Y, Zhang H (2018) Hydropower plant operation rules optimization response to climate change. Energy 160:886–897

Fallah-Mehdipour E, Bozorg-Haddad O, Loaiciga HA (2018) Calculation of multi-objective optimal tradeoffs between environmental flows and hydropower generation. Environ Earth Sci 77:453. https://doi.org/10.1007/s12665-018-7645-6

Fang R, Popole Z (2020) Multi-objective optimized scheduling model for hydropower reservoir based on improved particle swarm optimization algorithm. Environ Sci Pollut Res 27(12):12842–12850

Feng ZK, Liu S, Niu WJ, Li BJ, Wang WC, Luo B, Miao SM (2020) A modified sine cosine algorithm for accurate global optimization of numerical functions and multiple hydropower reservoirs operation. Knowl-Based Syst 208:106461

Garousi-Nejad I, Bozorg-Haddad O, Loáiciga HA (2016a) Modified firefly algorithm for solving multireservoir operation in continuous and discrete domains. J Water Resour Plan Manag 142(9):04016029

Garousi-Nejad I, Bozorg-Haddad O, Loáiciga HA, Mariño MA (2016b) Application of the firefly algorithm to optimal operation of reservoirs with the purpose of irrigation supply and hydropower production. J Irrig Drain Eng 142(10):04016041

Golfam P, Ashofteh P-S, Loáiciga HA (2021) Modeling adaptation policies to increase the synergies of water-climate-agriculture nexus under climate change. Environ Dev 37:100612. https://doi.org/10.1016/j.envdev.2021.100612

Hosseini-Moghari SM, Morovati R, Moghadas M, Araghinejad S (2015) Optimum operation of reservoir using two evolutionary algorithms: imperialist competitive algorithm (ICA) and cuckoo optimization algorithm (COA). Water Resour Manag 29(10):3749–3769

Jahandideh-Tehrani M, Bozorg-Haddad O, Loáiciga HA (2020) Application of particle swarm optimization to water management: an introduction and overview. Environ Monit Assess 192(5):1–18

Kennedy J, Eberhart R (1995) Particle swarm optimization. In: Proceedings of ICNN'95-international conference on neural networks. IEEE 4:1942–1948

Khalifeh S, Esmaili K, Khodashenas S, Akbarifard S (2020) Data on optimization of the non-linear Muskingum flood routing in Kardeh River using Goa algorithm. Data Brief 30:105398

Saremi Sh, Mirjalili S, Lewis A (2017) Grasshopper optimisation algorithm: theory and application. Adv Eng Softw 105:30–47

Sarzaeim P, Bozorg-Haddad O, Zolghadr-Asli B, Fallah-Mehdipour E, Loáiciga HA (2018) Optimization of run-of-river hydropower plant design under climate change conditions. Water Resour Manag 32(12):3919–3934

Xu Y, Mei Y (2018) A modified water cycle algorithm for long-term multi-reservoir optimization. Appl Soft Comput 71:317–332

Zeynali MJ, Shahidi A (2018) Performance assessment of grasshopper optimization algorithm for optimizing coefficients of sediment rating curve. AUT J Civ Eng 2(1):39–48

Zhang X, Liu P, Xu C-Y, Guo Sh, Gong Y, Li H (2019) Derivation of hydropower rules for multireservoir systems and its application for optimal reservoir storage allocation. J Water Resour Plan Manag 145(5):04019010